Finite Element Modeling for Dielectric Elastomer Actuators (DEA)

Luca Lampani and Paolo Gaudenzi
Sapienza, University of Rome
Department of Aerospace and Astronautical Engineering
Via Eudossiana 16/18 – 00184 Roma – Italy
lucalampani@yahoo.it, paolo.gaudenzi@uniroma1.it

ABSTRACT

A special sensor/actuator device based on dielectric elastomer (DEA) was studied and specialized to be used in applications for the space in the frame of the European Space Agency. The work illustrates the research project modeling procedure adopted to simulate the mechanical behavior of this material based on a finite element theory approach. The Mooney-Rivlin's hyperelastic and Maxwell's electrostatic models provide the theoretical basis to describe its electro-mechanic behavior. The validation of the procedure is performed through a numerical-experimental correlation between the response of two prototypes of sensor/actuator developed by the Risø Danish research center and the 3D finite element model simulations. An investigation concerning a possible application in the space environment of DEA actuators is also presented.

Keywords: EAP, DEA, dielectric elastomer, actuator, finite element

1. INTRODUCTION

For many years, electroactive ceramics, magnetostrictive materials and shape memory alloys have been the primary source of actuation materials for developing smart structural systems. Electroactive polymers (EAP) received relatively little attention due to their limited actuation capability. In recent years, effective EAP materials have emerged as a consequence of increased capability and potential. Sensors and actuators based on polymeric systems 1 are one of the most promising fields of "intelligent polymers", which is becoming more and more important also for their potential in artificial sensing and actuating systems in living organisms. Some practical applications have now started to be tested in engineering practice. Their main attractive characteristic is the operational similarity to biological muscles where a large displacement is induced under electrical excitation.

It is possible to group the several kinds of EAP in two categories depending if they are driven by electric field (electronic) or if they involve mobility of ions (ionic) (see Ref. 2 Sec.1.5 p.20). The attention is here focused on the dielectric elastomers, belonging to the first category, because of their capacity to induce large actuation strain, to have high energy density and fast speed of response. For these reasons these EAPs can offer a range of performances and characteristics that cannot be reproduced by other active materials.

The aim of this work is to establish a numerical model for the nonlinear constitutive behavior of dielectric elastomer actuators, by means of a finite element approach that is both iterative and incremental.

This study is a part of a ESA R&D project oriented to investigate the potential of the electroactive polymers in the frame of space systems, developed by a team of partners (Kayser Italia Srl, Risø Danish National Laboratory - Technical University of Denmark, Centro Piaggio - Pisa University, High Performance Space Structure Systems Gmbh, DLR German Aerospace Center).

In the framework of this partnership the authors have developed the simulation and design of the actuator/sensor systems embedded in a structural system to be used in the space environment

A model of the sensor/actuator ESA-C-4/II, developed by Risø, is proposed as application and its performances are correlated with the experimental ones. An overview of a space application in which this actuator is employed concludes the work.

2. WORKING PRINCIPLE OF DIELECTRIC ELASTOMER ACTUATORS (DEA)

This kind of EAP consists of an elastomer dielectric material that is coated on both sides with an expandable film that acts as a conducting electrode. When exposed to high electric fields, dielectric elastomers, such as silicones and acrylics, contract in the direction of the electric field lines, and expand perpendicularly to them. The stress state induced by the electromechanical coupling is known as the Maxwell stress (see Ref. 2 Sec.1.5.1.2 pp.23-24). The device is basically a flexible rubbery capacitor composed of two charged compliant parallel plates sandwiching a dielectric material. This effect is summarized in figure (Figure 1).

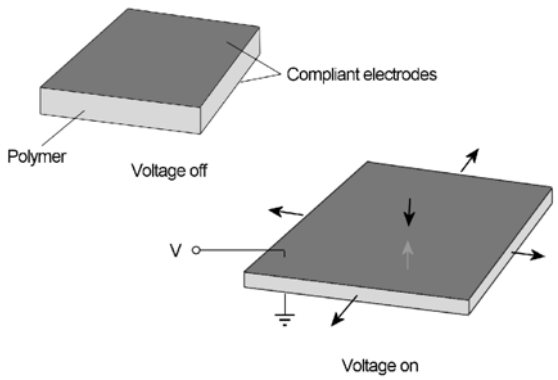

Figure 1. Working principle of dielectric elastomer actuators.

The polymers exhibit large strains, therefore the electrodes would have to be expandable as well. To this end compliant electrodes based on conductive particles in an elastomer matrix have been developed. Because the electrodes expand along with the plastic, they can maintain the electric field across the entire active region. Stretching the polymers prior to electric activation vastly improves the polymer performance. The prestretching orients the molecular chains along the plane, and makes it stiffer in that direction. To achieve this prestretching effect, the actuators contain an external bracing structure. Such prestretching may be anisotropic and thus may cause the effective elastic modulus to be anisotropic 3.

In order to obtain a numerical model that can simulate correctly the behavior of these actuators it is necessary to determine the following three points:

- the mechanical behavior of the polymer under electrical load;
- the electrical behavior and coupling with the mechanical one because the strongly dependence on a local thickness of the polymeric film;

- the prestretched configuration.

3. CONSTITUTIVE MODELS

Smart materials are used in the realization of smart structures for the purpose of developing actuation and sensing capabilities. In general the constitutive behavior of these materials couples their structural response (stress and strain) with other physical fields. The coupled behavior of smart materials can also be viewed as energy transduction between different physical fields (e.g. elastic and kinetic energy transformed into electrostatic energy or vice versa). For this reason smart structures are a typical example of a mechanical system governed by a multi-physics behavior.

In this way a mechanical stimulus can be transformed into a non-mechanical effect and, conversely, a non-mechanical stimulus can be converted into a mechanical effect. This is what happens in piezoelectric materials, where the electric behavior is coupled with the mechanical one due to the direct and converse piezoelectric effect. This effect enables the material to behave as an actuator or a sensor.

For the dielectric elastomers, the capability to sense is “indirect”; it means that a mechanical stimulus is not converted in an electrical signal but reading a variation of the physical characteristics as resistance or capacitance is needed for implementing the sensing.

Hyperelastic models provide a good basis for modeling the electric field and pre-strain dependencies of the transverse strain. From an engineering point of view, rubbers are homogeneous, isotropic materials that exhibit very large elastic strains (in a tensile test, a sample could reach ten times its original length) and they are almost incompressible. Moreover, one can observe from a tension test that the stress-strain behavior is strongly nonlinear. Rubber and rubber-like materials are usually modeled as incompressible hyperelastic materials.

Compressibility of rubbers and rubber-like materials is very low and, therefore, a model for an incompressible material is used. The nonlinear theory of elasticity is applied for the description of their mechanical behavior because structural components in the practice undergo large strain conditions. The finite-element method is suitable for the analysis of rubber and rubber-like materials provided that a nonlinear constitutive law and an iterative approach are used. In fact it is necessary to properly model the nonlinear stress-strain relations and take into account incompressible behavior of these materials, and the presence of large deformation.

3-1. Mechanical constitutive model

Consider a body at a generic time t, a fundamental measure of the deformation of the body is given by the *deformation gradient*, defined as:

$$ {}^{t}_{0}X = \left({}_{0}\nabla \ {}^{t}x^{T} \right)^{T} \tag{1} $$

where:

${}_{0}\nabla$: gradient operator

${}^{t}x$: coordinates at time t

The deformation gradient is used to measure the stretch of the material. In this calculation it is used the *right Cauchy-Green deformation* tensor:

$${}^t_0C = {}^t_0X^T \, {}^t_0X \tag{2}$$

A strain tensor that is valuable in finite element analysis is the *Green-Lagrange strain* tensor ${}^t_0\varepsilon$; this can be written in terms of Cauchy-Green deformation tensor as:

$${}^t_0\varepsilon = \frac{1}{2}\left({}^t_0C - I\right) \tag{3}$$

The energy conjugate stress measure to use with the Green-Lagrange strain tensor is the *second Piola-Kirchhoff stress* tensor ${}^t_0S$ (see 4 Sec.6.2.2 p.515).

Hyperelastic material models assume that materials response is isotropic and isothermal. This assumption allows that the strain energy potentials are expressed in terms of strain invariants or principal stretch ratios. Except as otherwise indicated, the materials are also assumed to be nearly or purely incompressible. Material thermal expansion is also assumed to be isotropic.

The constitutive behavior of hyperelastic materials are usually derived from the strain energy potentials. The isotropic hyperelastic effects are mathematically described by specifying the dependence of the strain energy density (per unit original volume) W on the Green-Lagrange strain tensor.

Depending on the specific material model used, several forms of strain energy potential, such as Neo-Hookean, Mooney-Rivlin, Polynomial Form, Ogden Potential, Arruda-Boyce, Gent, and Yeoh are available (see 5 Sec.3.8 p.325).

The use of Mooney-Rivlin model for mechanical response is justified by the strain range of the DEA materials used in this study. As it will be shown in the next section, for a stretch of 100% this model will allow a good fit of the constitutive behavior.

The conventional Mooney-Rivlin model 4 is described by the strain energy density per unit original volume:

$${}^t_0\widetilde{W} = C_1\left({}^t_0I_1 - 3\right) + C_2\left({}^t_0I_2 - 3\right) \qquad {}^t_0I_3 = 1 \tag{4}$$

where C_1 and C_2 are material constants and the invariants ${}^t_0I_i$ are given in terms of the components of the Cauchy-Green deformation tensor:

$$\begin{aligned} {}^t_0I_1 &= {}^t_0C_{kk} \\ {}^t_0I_2 &= \frac{1}{2}\left[\left({}^t_0I_1\right)^2 - {}^t_0C_{ij}\,{}^t_0C_{ij}\right] \\ {}^t_0I_3 &= \det {}^t_0C \end{aligned} \tag{5}$$

The description in Eq. (4) assumes that the material is totally incompressible (since ${}^t_0I_3 = 1$). A better assumption is that the bulk modulus is several thousand times large as the shear modulus, which then means that the material is almost incompressible. This assumption is incorporated by dropping the restriction that ${}^t_0I_3 = 1$ and including a hydrostatic work term W_H in the strain energy function to obtain

$${}^t_0\widetilde{\widetilde{W}} = C_1\left({}^t_0I_1 - 3\right) + C_2\left({}^t_0I_2 - 3\right) + W_H\left({}^t_0I_3\right) \tag{6}$$

However, this expression cannot be used directly in the displacement/pressure formulations because all the three terms contribute to the pressure. To obtain an appropriate expression, it is possible to define the reduced invariants:

$$
\begin{aligned}
{}^{t}_{0}J_1 &= {}^{t}_{0}I_1\left({}^{t}_{0}I_3\right)^{-\frac{1}{3}} \\
{}^{t}_{0}J_2 &= {}^{t}_{0}I_2\left({}^{t}_{0}I_3\right)^{-\frac{2}{3}} \\
{}^{t}_{0}J_3 &= \left({}^{t}_{0}I_3\right)^{-\frac{1}{2}}
\end{aligned}
\tag{7}
$$

so that in conclusion:

$${}^{t}_{0}\overline{W} = C_1\left({}^{t}_{0}J_1 - 3\right) + C_2\left({}^{t}_{0}J_2 - 3\right) + \frac{1}{2}\kappa\left({}^{t}_{0}J_3 - 1\right)^2 \tag{8}$$

where κ is the bulk modulus.

We note that in this description

$${}^{t}\overline{p} = -\kappa\left({}^{t}_{0}J_3 - 1\right) \tag{9}$$

With the knowledge of how the strain energy density *W* depends on the Green-Lagrange strain tensor (through the invariants or stretches), the 2nd Piola-Kirchhoff stress tensor is evaluated using:

$$S_{ij} = \frac{1}{2}\left(\frac{\partial W}{\partial \varepsilon_{ij}} + \frac{\partial W}{\partial \varepsilon_{ji}}\right) \tag{10}$$

and the incremental material elastic tensor is evaluated using the following expression:

$$C_{ijrs} = \frac{1}{2}\left(\frac{\partial S_{ij}}{\partial \varepsilon_{rs}} + \frac{\partial S_{ij}}{\partial \varepsilon_{sr}}\right) \tag{11}$$

3-2. Electrical constitutive model

The mechanical driving force of the dielectric elastomer actuator derives from the well known Coulomb charge attraction effect. When a capacitor is charged by application of an electric field, positive charges reside on one electrode, balanced by negative charges on the other electrode. The compliance of the elastomer allows the charges to move closer by squeezing the capacitor. Volume conservation forces the elastomer to expand transversely to electric field, increasing the area of electrodes. This increase lets charges on one electrode move further apart, lowering the internal energy of the charges. This energy can be converted to mechanical energy (strain, stress) through a number of mechanisms, the simplest being through the Maxwell stress, which all materials exhibit.

The generic expression of Maxwell stress for dielectric material is:

$$\sigma_{ij} = \varepsilon_R \varepsilon_0 E_i E_j - \frac{1}{2}\varepsilon_R \varepsilon_0 E^2 \delta_{ij} \tag{12}$$

where

- E is the electric field that can be expressed as gradient of electric potential $E = -\nabla\phi$
- ε_R is the relative permittivity of the material
- ε_0 is the permittivity of vacuum
- δ_{ij} is the Kronecker delta.

We can observe that the stress depends upon the applied electric field to second order; writing the electric field as E=V/z, it is clear that the thickness of the insulating elastic film does enter, and in fact the stress is inversely proportional to the square of thickness 6 7.

The electric flux density in the material can be expressed as:

$$D_i = \varepsilon_{ij} E_j \tag{13}$$

where $\varepsilon=\varepsilon_R\ \varepsilon_0$ is the permittivity of the material.

4. FINITE ELEMENT APPROACH

The above mechanical and electrical constitutive equations are rearranged now to represent the coupled behavior of the material.

$$\begin{cases} \sigma_{ij} = \sigma_{ij\ Mooney-Rivlin} + \sigma_{ij\ Maxwell} & (14) \\ D_i = \varepsilon_{ij} E_j & (15) \end{cases}$$

In the above equations the sensing behavior is not accounted for. In eq. (14) Maxwell stress is the coupling term between mechanical and electric field; in eq. (15) we have only electric variables, due to the fact sensing effects are neglected.

Let us now address the nonlinear nature of the response and propose an iterative finite element procedure for the analysis of piezoelectric continua, as also proposed in Ref. 8. From a computational viewpoint one of the key advantages of this iterative approach is that already existing finite element programs that solve classical solid mechanics problems and field problems, like heat transfer, can directly be used in a reliable way providing that the constitutive law is modified. It is so possible to include material nonlinearities in the procedure as discussed below.

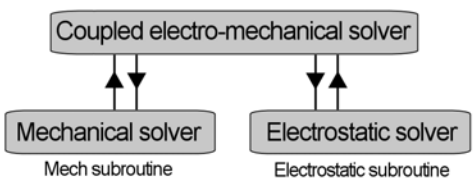

Figure 2. Numerical solver approach.

In order to establish a general solution scheme for nonlinear problems the use of incremental equilibrium equations is necessary; so, we have to use a procedure that is both iterative and also incremental, dealing at every iteration with the mechanical or electrical equilibrium.

The figure (Figure 2) summarizes the numerical solver approach. The governing equations for the electric field is first solved and the values of the electric variables are given as an entry to the mechanical solver that provides a mechanical solution that is, in turn, given back to the electric solver. This procedure iterates until a convergence is reached for both mechanical and electrical variables. The mechanical solver accounts, for the nonlinear behavior described before, and provide further iterations, as described in the next section.

4-1. Mechanical subroutine

Eq. (14) is solved using a coupled mech-solver and user supplied code with the following scheme:

$$^{(k)}\sigma_{ij} = {}^{(k-1)}\sigma_{ij\ Mooney-Rivlin}(W) + {}^{(k-1)}\sigma_{ij\ Maxwell}(E) \tag{16}$$

The mechanical constitutive subroutine executes the following operations:

1. Calculate deformation gradient, its inverse and invariants
2. Calculate first derivatives of invariants and reduced invariants respect to strain components
3. Compute first derivatives of the strain energy density W with respect to reduced invariants
4. Calculate 2° Piola-Kirchhoff stresses
5. Calculate Maxwell stresses in local system
6. Transform Maxwell stresses in global system
7. Sum of Piola-Kirchoff and Maxwell stresses
8. Compute second derivatives of the invariants and reduced invariants with respect to strain components
9. Calculate second derivatives of the strain energy density W with respect to reduced invariants
10. Calculate tangent constitutive tensor to update the stiffness matrix

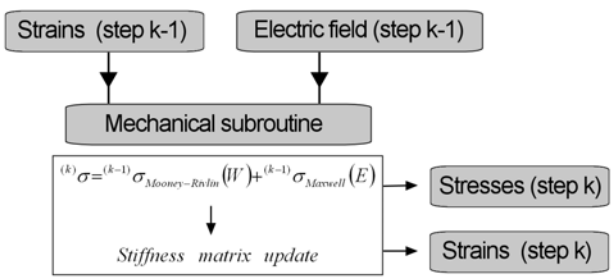

Figure 3. Mechanical subroutine.

4-2. Electrostatic subroutine

Eq. (15) is solved using ADINA thermal-solver and user supplied code with the following scheme:

$$^{(k)}D_i = \varepsilon_{ij}\,{}^{(k-1)}E_j \tag{17}$$

The thermal/electrostatic constitutive subroutine executes the following operations:

1. Calculates electric displacements
2. Calculates tangent constitutive tensor to update the permittivity matrix

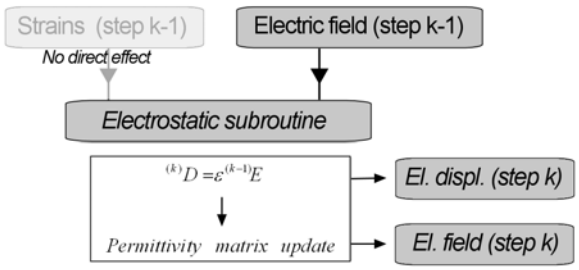

Figure 4. Electrostatic subroutine.

4-3. Characterization of the constitutive equations

In order to validate the proposed finite element approach, a characterization of the mechanical behavior of the Elastosil RTV E625, a silicone material used for the fabrication of the actuators considered in this work, is studied. The model used for the simulation of the tensile test is a rubber specimen; it allows to calibrate the constants of the hyperelastic material according to the Mooney-Rivlin theory to fit the experimental behavior 9. At this aim it is necessary to find the proper material constants (

Table 1). The Figure 5 shows the best fitting operated on the stretch-stress curve with a good agreement below a stretch value of 1.5.

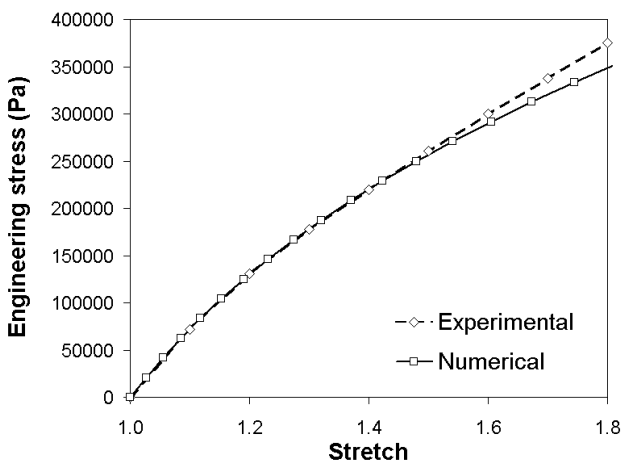

Figure 5. Numerical fitting of Elastosil RTV E625 characteristics.

Elastosil RTV E625 material characteristics:

$$\sigma = 2\left(C_1 + \frac{C_2}{\lambda}\right)\left(\lambda - \frac{1}{\lambda^2}\right)$$ Mooney-Rivlin theory

C_1 = 100 kPa
C_2 = 33 kPa

Table 1. Material properties.

The validation of the electrostatic behavior is performed coupled with the mechanical one. Prototypes of sensor/actuator, explained more in detail in the next chapter, are taken as benchmark case. A second iteration to characterize the mechanical behavior is performed on a finite element model of the actuator in order to obtain a fine tune of the constants of the material taking in account the presence of the compliant electrodes.

In

Figure 6 the coupled electro-mechanical behavior of the actuator is depicted. The voltage is applied on a pre-stretched configuration, to increase the efficiency of the actuation effect. The graph highlights, with an example, the strong non-linearity of the stress (Mooney-Rivlin + Maxwell) function of the electric field.

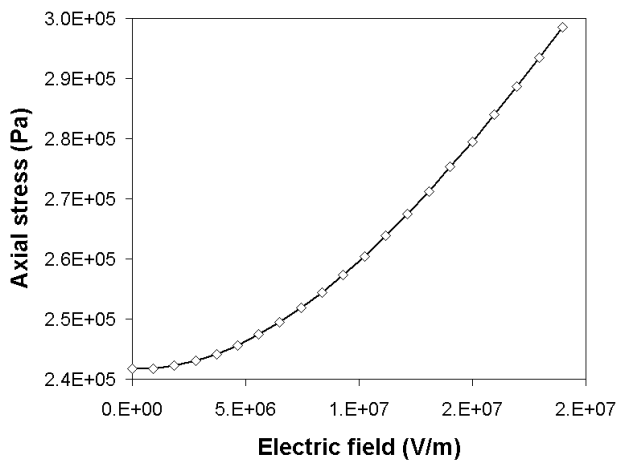

Figure 6. Coupled electro-mechanical behavior of a Elastosil RTV E625 based actuator.

5. Risø sensor/actuator ESA-C-4

5-1. The prototype of the ESA-C-4/I

The ESA-C-4/I is a dielectric elastomer actuator with smart compliant electrodes (
Figure 7). This prototype is a multilayered structure (five layers), 100mm long, 70mm wide.

Four sheets act as actuator and one as sensor. The electrode areas are evaporated on the five films (37 micron thin each) of Elastosil RTV E625 silicone from Wacker 3 10 11. Each electrode is produced by evaporation of Ag for a thickness of 75nm. Multilayers are glued together using a conductive silicone, Elastosil LR3132. The connectors extend 2.5mm outside the electrode area; the electrical leads are embedded in a connection pad of one layer.

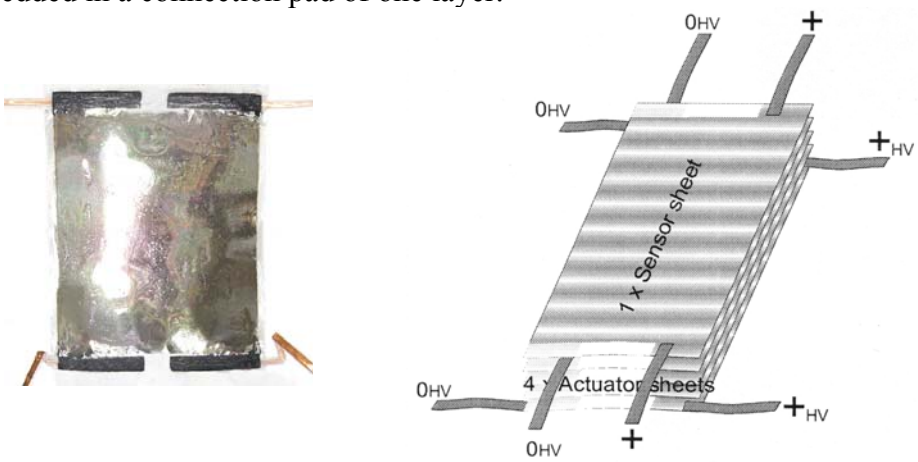

Figure 7. Risø sensor/actuator ESA-C-4/I.
(Courtesy of Risø Danish National Laboratory)

5-2. The prototype of the ESA-C-4/II

The ESA-C-4/II (

Figure 8) is similar to the previous one. This prototype is a multilayered structure (four layers), 100mm long, 70mm wide. Each sheet acts as both sensor and actuator, and they consist of two 5mm wide sensor (through the measurement of the capacity) parts side-by-side with a 55mm wide actuator part.

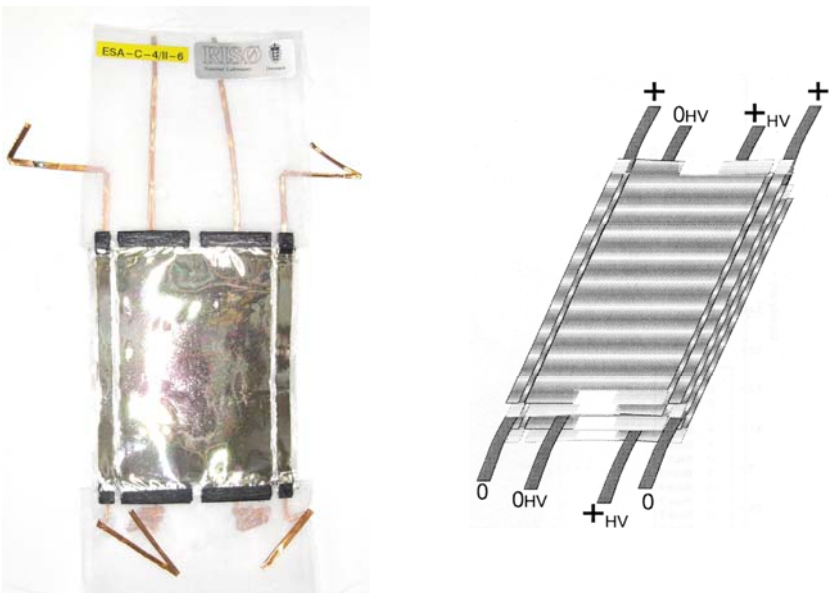

Figure 8. Risø sensor/actuator ESA-C-4/II.
(Courtesy of Risø Danish National Laboratory)

5-3. The experimental set-up and the finite element model

In the experimental set-up and in the numerical simulation on the 3D model the actuator is in vertical position clamped at one end and loaded by the weight of a mass attached to it. A rigid bar is attached to the free end in order to distribute the stress homogeneously. The main information of the finite element models is summarized in Table 2.

ESA-C-4/I	***ESA-C-4/II***
14198 nodes.	14685 nodes.
Element group 1: actuator material 1350 3D solid elements 27 nodes. Element group 2: sensor material 270 3D solid elements 27 nodes. Element group 3: pad material 60 3D solid elements 27 nodes. Element group 4: clamp 30 shell elements 9 nodes.	Element group 1: actuator material 720 3D solid elements 27 nodes. Element group 2: sensor material 688 3D solid elements 27 nodes. Element group 3: pad material 128 3D solid elements 27 nodes. Element group 4: clamp 64 shell elements 9 nodes.
1710 elements total.	1600 elements total.
Material characteristics:	Material characteristics:
Actuator / sensor layers: Elastosil RTV E625 + electrodes C_1 = 185 kPa C_2 = 33 kPa Permittivity $\varepsilon = 3.28 \times 10^{-11}$ F/m	Actuator / sensor layers: Elastosil RTV E625 + electrodes C_1 = 215 kPa C_2 = 33 kPa Permittivity $\varepsilon = 3.72 \times 10^{-11}$ F/m
Pads: Elastosil RTV E625 C_1 = 100 kPa C_2 = 33 kPa	Pads: Elastosil RTV E625 C_1 = 100 kPa C_2 = 33 kPa

Table 2. Finite element model main information.

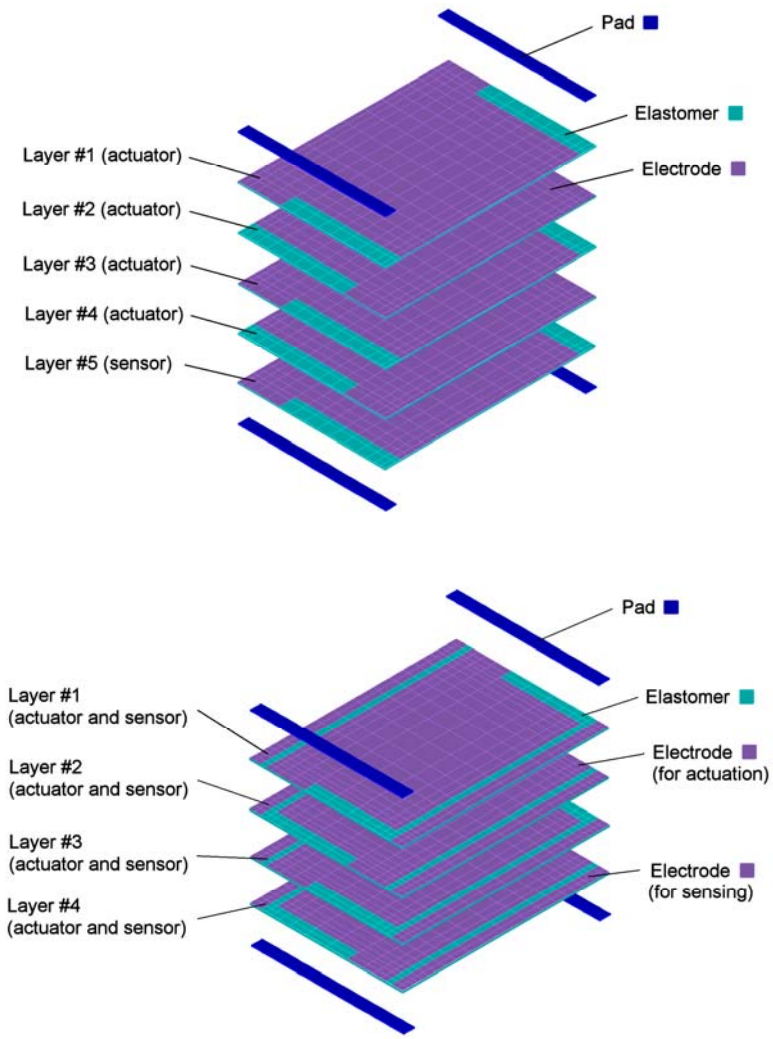

Figure 9. Exploded views of the finite element models sensor/actuator ESA-C-4/I (up) and ESA-C-4/II (down).

The best performances of the actuators are obtained in a pre-stressed condition. In particular the optimal pre-stress is achievable with a load mass of 50 g/layer, therefore 250 g for the first actuator and 200 g for the second, to which a force of 2.453 N and 1.962 N corresponds. A power supply provides the electrodes of a continuous voltage up to 2500 V. This is the electrostatic limit of the actuator seen as a condenser. Beyond this threshold some discharge induces the breakdown of the system.

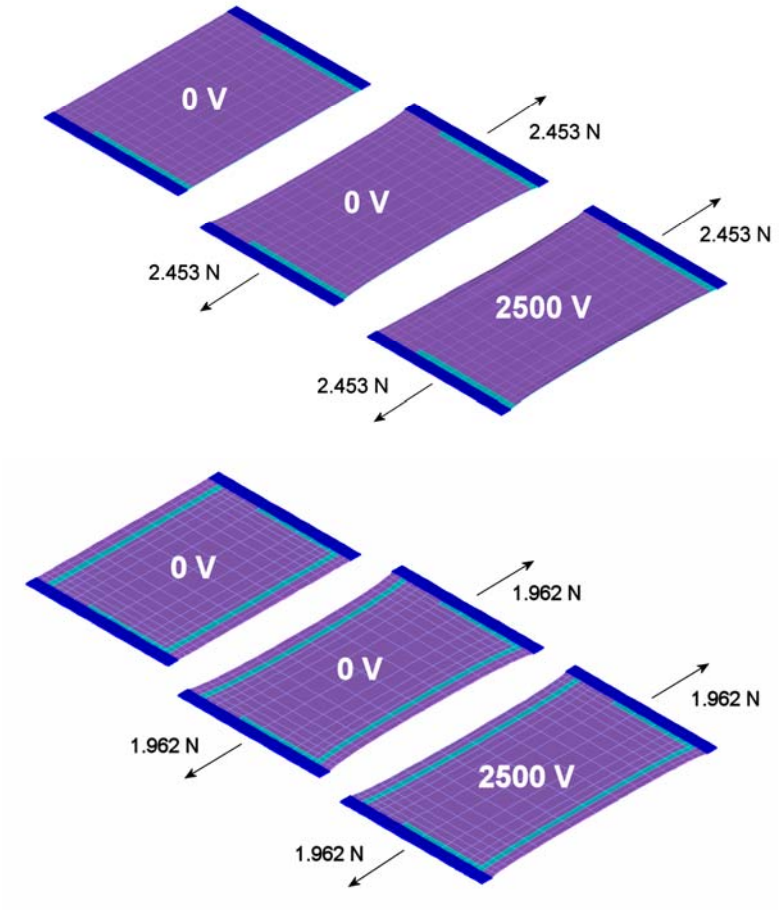

Figure 10. Finite element model of the sensor/actuator ESA-C-4/I (up) and ESA-C-4/II (down).

The test is then composed of two phases, resumed in the Figure 10.

- The first is the pre-loading phase: no actuation is present. An increasing tensile load from 0 to the optimal force is applied. The first actuator extends of 10.9 mm and the second of 10.5 mm, as depicted in the first row of Figure 11. The stretching is quite linear; only the mechanical hyperelastic behavior is present.
- The second is the actuation phase: starting from the pre-stressed configuration reached at the end of the previous phase and maintaining the loading force of 1.962 N for the first actuator and 2.453 N for the second one, an increasing voltage from 0 to 2500 V is applied to the electrodes. The first actuator extends of 5.9 mm and the second of 6 mm (second row of Figure 11). The stretching is non-linear; both the mechanical hyperelastic and electro-mechanical behavior are present.

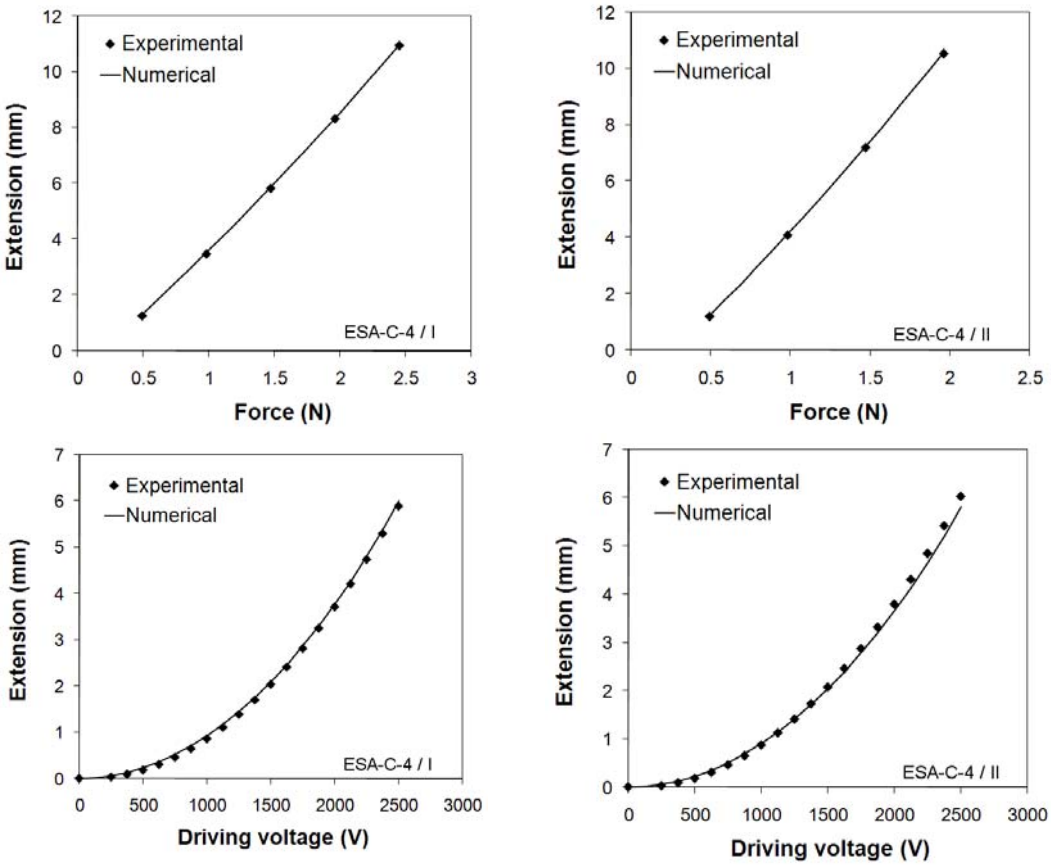

Figure 11. Behavior of the actuator with preload and voltage 12.

The mesh is refined to a level that allows simulating in a good way the stretching along the thickness. This stretching has a strong influence on the electric field and then on the actuation behavior (Figure 12).

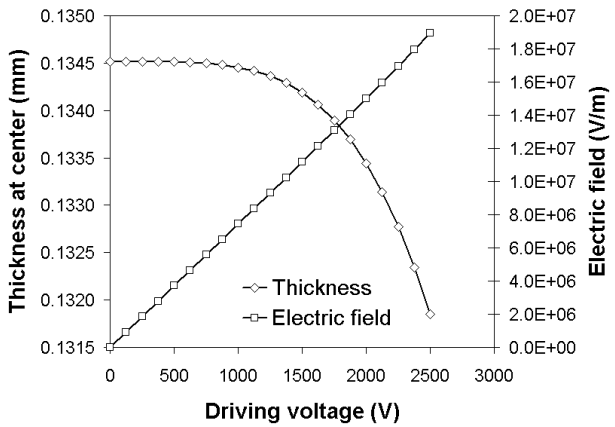

Figure 12. Thickness at center of the actuator and electric field vs. driving voltage.

A reasonable agreement is reached for the characterization of the material. The next step is to include this numerical material model in the frame of a breadboard developed to demonstrate the suitability of the DEA actuators in a real case of space structure.

7. A SPACE APPLICATION FOR THE ESA-C-4/II: CFRP DEPLOYABLE/INFLATABLE BOOM

7-1. The breadboard

The DEA actuators are characterized by large stroke and low force. The work density, the product of stress and strain, is however among the highest of all electromagnetically driven actuator technologies. In order to utilize it efficiently, e.g. in order to damp large-scale vibrations, it is necessary to allow the actuator to work over its full stroke range. In order to study DEAs have been used to damp the structural vibration of a deployable/ inflatable boom (Figure 13).

Figure 13. Breadboard of the deployable/inflatable boom with DEAs 13.
(Courtesy of High Performance Space Structure Systems Gmbh)

The boom has a nominal length of 3 m and a diameter of 134 mm. It is made in CFRP: two layers of carbon fiber prepregs are applied onto an inflated nylon hose. The inner layer is made from a 45° plain weave carbon fiber prepreg with a mass of 95g/m² while the outer layer is made from a unidirectional CF prepreg with a mass of 150g/m². Thickness of the laminate is 0.6 mm (+/- 45°ply: 0.17 mm, UD-ply 0.43 mm). Two flanges in aluminum, 3.5kg of weight, are used as end cap. One of them provides the clamping to the ground, the other represents a tip mass as a generic payload. The four sensor/actuators are positioned at 0.5, 1.0, 1.5 and 2.0m from the clamped base.

7-2. The working principle

Here, the embedding structure supplies the pre-load: the inner walls of the boom have low flexural stiffness and the actuator is stretched out between them (Figure 14); hence the boom profile is compressed in the direction of the actuator and balances the actuators contractile force.

Activating the actuator will extend it and allow the cross-sectional profile of the boom to return to its natural configuration. Upon discharging, the actuator will force the structure back in the initial compressed configuration. The actuator works over its full stroke, and the induced local change of the booms longitudinal bending stiffness can be utilized to damp large-scale vibrations. By varying the

cross-sectional shape of the boom at certain points, the actuators provide a variation of the bending stiffness of the section. This effect creates the actuation effect in the structural behavior of the boom.

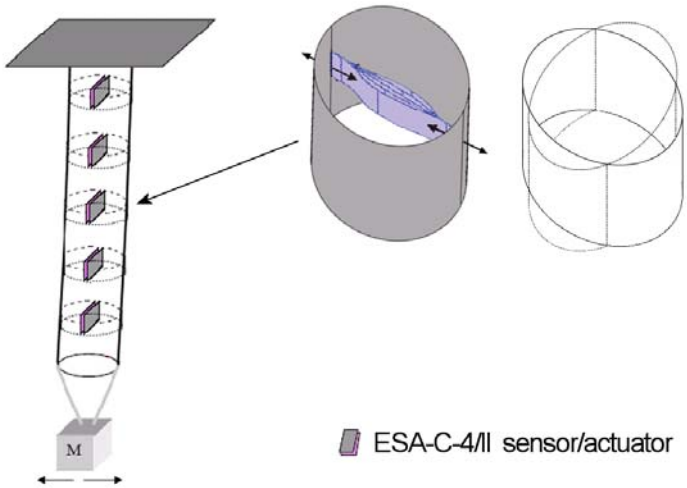

Figure 14. Working principle of the boom with DEAs for vibration control.

7-3. Finite element model

The model of the boom, with the four ESA-C-4/II sensor/actuators integrated (Figure 15) reproduces the experimental breadboard. The boom structure is modeled by multilayered shell elements.

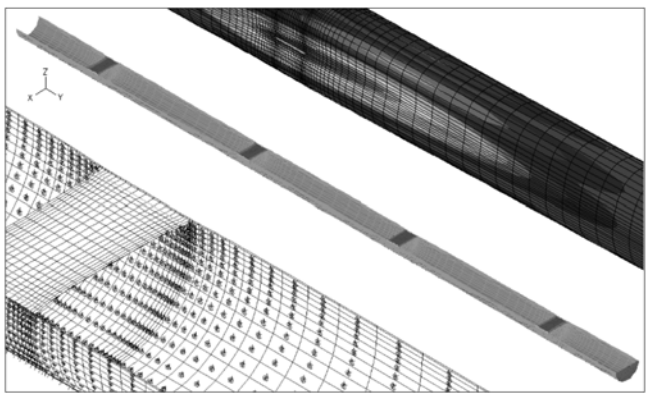

Figure 15. FE model of the boom with DEAs for vibration control 14.

In order to produce the shrinkage of the section of the boom, the actuator is pre-stretched before to be attached to the skin of the boom. At the equilibrium, also the section of the boom is pre-loaded. The numerical sequence adopted is to stretch the actuator to the diameter as first step, then to attach its ends (provided of fabric end-connectors) to the skin of the boom, and to release gradually the body to reach the configuration of equilibrium.

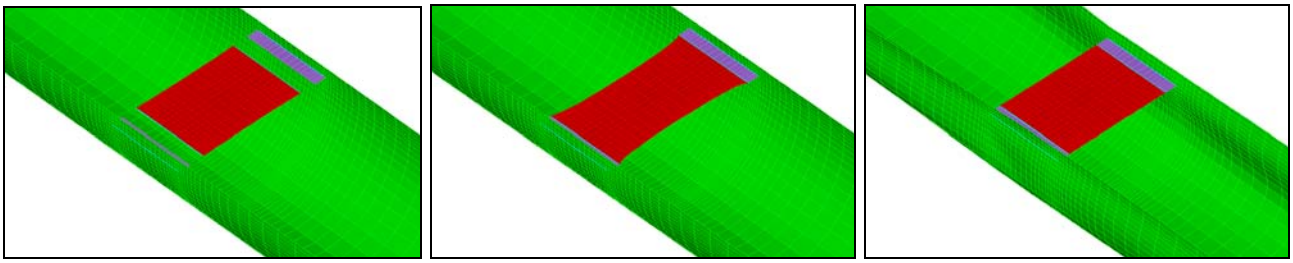

Figure 16. Simulation of insertion sequence of the actuators into the boom structure.

A logic of control is developed and applied in order to reduce the amplitude of the vibrations of the system. We apply a pull-release excitation to the free end to induce a bending oscillation mainly on first mode. This is the input. The output is acquired from an accelerometer and a position sensor on the free end. In the Figure 17 the time response of the position and the acceleration are reported with and without the application of the control.

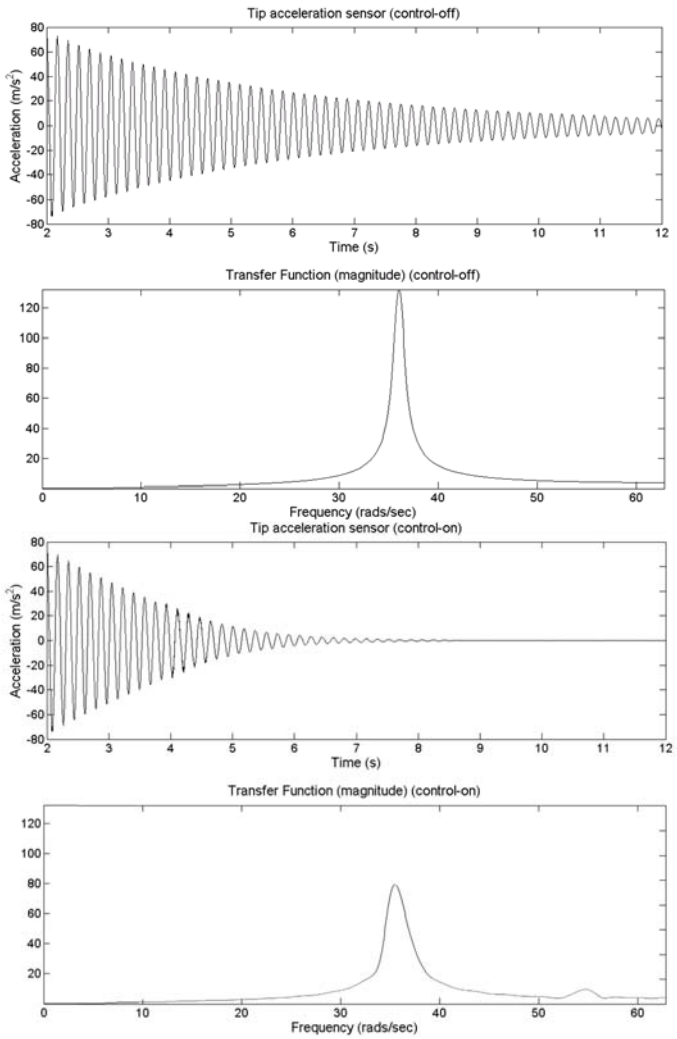

Figure 17. Time history and transfer function of the acceleration at the free end of the boom with and without control.

From the picture the effect of the actuation on the amplitude of the acceleration at the free end of the boom is reported.

8. CONCLUSIONS

A procedure to simulate the behavior of the dielectric elastomer actuators through a finite element approach has been proposed. A constitutive model of the dielectric elastomer Elastosil RTV E625 has been derived from traction test and a good fitting with the experimental results has been obtained. The actuation capabilities of a three-dimensional FE model have been compared with two Risø's prototypes and validated with good agreement. The interaction of this actuator with a structure has been then tested by analyzing the behavior of a breadboard structure.

ACKNOWLEDGMENTS

This work has been developed in the context of the research project of ESA/ESTEC "Electro-active polymers" contract no. 18548/04/NL/PA directed by Kayser Italia with which the Dipartimento di Ingegneria Aerospaziale e Astronautica, Sapienza – Università di Roma, collaborated.

REFERENCES

1. Osada Y.,De Rossi D.E. "Polymer sensors and actuators". Springer, 2000
2. Bar-Cohen, Y.(Ed.). "Electroactive Polymer (EAP) Actuators as Artificial Muscles" - Reality, Potential and Challenges. SPIE Press, Vol. PM98, 2001.
3. Benslimane M., Gravesen, P., Sommer-Larsen P. "Mechanical properties of dielectric elastomer actuators with smart metallic compliant electrodes". Smart Structures and Materials 2002: Electroactive Polymer Actuators and Devices (EAPAD) Edited by Bar-Cohen, Yoseph. Proc. SPIE Vol. 4695, p. 150-157
4. Bathe K.J. "Finite Element Procedures". Prentice Hall, 1996
5. "Theory and Modeling Guide", Volume I: ADINA, ADINA R&D, Inc., Report ARD 04-7, September 2004
6. Kofod G., Kornbluh R., Pelrine R., Sommer-Larsen P. "Actuation response of polyacrylate dielectric elastomers". Journal of Intelligent Material Systems and Structures, Vol.14 December 2003.
7. Sommer-Larsen P., Larsen A. L. "Materials for dielectric elastomer actuators". Smart Structures and Materials: Electroactive Polymer Actuators and Devices (EAPAD). Edited by Bar-Cohen, Yoseph. Proceedings of the SPIE, Volume 5385, pp. 68-77, 2004.
8. Gaudenzi P., Bathe K. J. "An iterative finite element procedure for the analysis of piezoelectric continua". Journal of Intelligent Material Systems and Structures, Vol. 6, 1995, 266-273.
9. Project "Electro-active Polymers", ESA/ESTEC contract 18548/04/NL/PA, report RIS-EAP-TR-01 pag.36
10. Sommer-Larsen P., Kofod G., Shridhar M.H., Benslimane M., Gravesen P. "Performance of dielectric elastomer actuators and materials". Proc. SPIE Vol. 4695, p. 158-166, Smart Structures

and Materials 2002: Electroactive Polymer Actuators and Devices (EAPAD), Yoseph Bar-Cohen; Ed.
11. Kofod G., Sommer-Larsen P. “Silicone dielectric elastomer actuators: Finite-elasticity model of actuation”. Journal: Sensors and Actuators A:Physical. Vol./Iss.:122, 2 , 2005
12. Project “Electro-active Polymers”, ESA/ESTEC contract 18548/04/NL/PA, report RIS-EAP-RP2113-01 pagg.8,14
13. Project “Electro-active Polymers”, ESA/ESTEC contract 18548/04/NL/PA, report EAP-HPS-RP-003 pagg.4-4, 4-19.
14. Project “Electro-active Polymers”, ESA/ESTEC contract 18548/04/NL/PA, report EAP-DIAA-RP-01 pag.21